44th AIAA/ASME/SAE/ASEE Joint Propulsion Conference & Exhibit
21 - 23 July 2008, Hartford, CT

AIAA 2008-4924

Efficacy of Electron Mobility Models in Hybrid-PIC Hall Thruster Simulations

Richard R. Hofer,[*] Ira Katz,[†] Ioannis G. Mikellides,[‡] Dan M. Goebel,[§] Kristina K. Jameson,[**]
Regina M. Sullivan,[††] and Lee K. Johnson[‡‡]
Jet Propulsion Laboratory, California Institute of Technology, Pasadena, CA 91109

The cross-field electron mobility in Hall thrusters is known to be enhanced by wall collisionality and turbulent plasma fluctuations. Although progress has been made in understanding the plasma-wall interaction and instabilities responsible for the anomalous transport, a predictive model based on the underlying physics of these processes has yet to emerge. Hybrid-PIC simulations of the Hall thruster have typically depended on semi-empirical models of the mobility to provide sufficient electron current to match experimental results. These models are capable of qualitatively predicting the plasma response over a wide range of operating conditions, but have limited quantitative capabilities unless they are calibrated with experimental data. The efficacy of several electron mobility models in reproducing the plasma response of a 6 kW laboratory Hall thruster are assessed. With respect to a two-region mobility model that is frequently reported in the literature, a three-region model for the mobility is shown to significantly improve the agreement with experimentally measured profiles of the plasma potential and electron temperature.

[*] Technical Staff Member, Electric Propulsion Group, Propulsion and Materials Engineering Section, 4800 Oak Grove Dr., MS 125-109, Pasadena, CA 91109, richard.r.hofer@jpl.nasa.gov. Senior Member AIAA.

[†] Principal Engineer and Group Supervisor, Electric Propulsion Group, Propulsion and Materials Engineering Section. Senior Member AIAA.

[‡] Senior Engineer, Electric Propulsion Group, Propulsion and Materials Engineering Section. Senior Member AIAA.

[§] Senior Research Scientist, Propulsion and Materials Engineering Section. Senior Member AIAA.

[**] Academic Part-Time Staff, Electric Propulsion Group, Student Member AIAA.

[††] Ph.D. Candidate, Engineering and Applied Sciences, Student Member AIAA.

[‡‡] Senior Engineer, Propulsion and Materials Engineering Section. Senior Member AIAA.

Nomenclature

B_r = radial magnetic field component
D = discharge chamber mid-diameter
$\vec{E}$, E_z = electric field vector and its axial component
E_i = ionization potential
$\dot{E}_w$ = wall energy loss rate
f = fraction for applying turbulence collision frequency
I_b, I_d, I_e, I_i = current of the ion beam (ΣI_i), the discharge (I_b+I_e), the electrons, and the i[th] ion species
$I_{sp,a}$ = anode specific impulse
i = ion charge-stage index (1, 2, 3, etc.)
$\vec{j}_b$, j_{bz} = ion current density vector and its axial component
$\vec{j}_e$, j_{ez}, $j_{e\theta}$ = electron current density vector and its axial and azimuthal components
ℓ = magnetic field line index (1, 2, etc.)
L = discharge chamber length
$\dot{m}_a$, $\dot{m}_b$, $\dot{m}_c$, $\dot{m}_i$, $\dot{m}_t$ = mass flow rate of the anode, the ion beam ($\Sigma\dot{m}_i$), the cathode, the i[th] ion species, and the total ($\dot{m}_a + \dot{m}_c$)
m_e, m_{xe} = electron and xenon atom mass
N = total number of ion species
n_e, n_n = number density of electrons and neutrals
$\dot{n}_i$ = ionization rate of ions
P_d, P_{jet}, P_{mag} , P_t = power of the discharge ($V_d I_d$), the jet (or beam) ($T^2/2\dot{m}_t$), the electromagnet coils, and the total input ($P_d + P_{mag}$)
p = vacuum chamber pressure
$Q_{e\text{-}n}$ = electron-neutral collision cross-section
$\vec{q}_e$ = heat flux vector
r = radial position
S_i = inelastic energy loss term due to ionization and excitation
T = thrust
t = time
T_e = electron temperature
$\vec{u}_e$ = electron velocity vector
V_a, V_d, V_l = acceleration voltage (V_d - V_l), discharge voltage, ion loss voltage
V_p = plasma potential
v_{ExB} = ExB drift velocity, ~ E_z/B_r
v_i = velocity of the i[th] ion species
Z_i = charge-state of the i[th] ion species (1, 2, 3, etc.)
z = axial position
α_c, α_e, α_p = turbulence coefficient for the channel (region I), exit (region II), and plume (region III)
χ = position along a magnetic field line
ΔA = magnetic field line centered area element along the wall
ΔV = magnetic field line centered volume element
δ_w = secondary electron emission yield
ε = electron current fraction, I_e/I_d
ϕ = azimuthal position
Γ_{brQ} = radial ion flux at the sheath edge
η_a, η_b, η_c, η_d, η_{mag}, η_m, η_q, η_v, η_t = anode efficiency, current utilization efficiency, cathode efficiency ($\dot{m}_a/\dot{m}_t$), plume divergence utilization efficiency, electromagnet coil efficiency (P_d/P_t), mass utilization efficiency, charge utilization efficiency, voltage utilization efficiency, total efficiency
φ = Dugan's ionization cost including excitation
$\mu_{e\perp}$ = cross-field electron mobility

ν_e, ν_b, ν_{ei}, ν_{en}, ν_w = total effective electron collision frequency, effective electron collision frequency due to turbulence, electron-ion collision frequency, electron-neutral collision frequency, electron-wall collision frequency

θ = plume divergence half-angle

ξ = exchange ratio, $m_{xe} I_d / \dot{m}_a e$

Ω_e = electron Hall parameter, $\omega_{ce}/\nu_e = j_{e\theta}/j_{ez}$

Ω_i = current fraction of the i^{th} ion species, I_i/I_b

ω_{ce} = electron cyclotron frequency

I. Introduction

COMMERCIAL electric propulsion systems are now being considered as a cost effective solution for competitively awarded science missions such as the NASA Discovery and New Frontiers programs [1,2]. Many of the missions being studied would require wider power throttling capabilities and longer thruster life compared to commercial applications. These differences can be addressed through a combination of delta-qualification testing and modeling [1,2]. An electric propulsion life-modeling program has been ongoing at the Jet Propulsion Laboratory (JPL) for the past several years in an effort to establish a thruster life qualification capability for ion thrusters, hollow cathodes, and Hall thrusters [3-6]. The aim of this program is to provide NASA with a set of physics-based modeling tools that can be used to address the qualification gaps between ground testing and actual mission requirements in order to decrease or eliminate the cost and time required to assess thruster service life through time-consuming and expensive life testing.

Plasma and erosion models of Hall thruster discharge chambers are currently under development at JPL [4]. The models have been applied to a variety of different thrusters, including the SPT-100, BPT-4000, and several NASA thrusters. The plasma model is based on a JPL modified version of HPHall-2 [7,8]. HPHall is an axisymmetric simulation of the Hall thruster employing a hybrid fluid/particle-in-cell (hybrid-PIC) numerical approach to simulate the evolution of the plasma inside the discharge chamber and near-field plume. HPHall, originally developed by Fife and Martínez-Sánchez [7], was upgraded to HPHall-2 by Parra and Ahedo [8]. Additional upgrades to the code, including the development of an erosion submodel, have been reported by our group in Ref. [4,9-12].

In this paper, we assess the efficacy of several electron mobility models to qualitatively and quantitatively reproduce the plasma response of a 6 kW laboratory Hall thruster. The details of the mobility models are presented in section II. Section III presents recent upgrades to the code and section IV discusses inputs used for the simulations and experimental results. Section V presents results from the mobility models compared with experiment. Section VI discusses the accuracy of the models followed by a final comparison between the model that most accurately reproduces the experiment data.

II. Cross-Field Electron Mobility Modeling

The cross-field electron mobility in Hall thrusters is well described by

$$\mu_{e\perp} = \frac{e}{\nu_e m_e}\left(\frac{1}{1+\Omega_e^2}\right), \tag{1}$$

where ν_e is the total effective electron collision frequency, Ω_e is the electron Hall parameter, and the rest of the symbols have their usual meaning. Wall collisions and turbulent plasma fluctuations, so-called "anomalous" transport mechanisms, enhance the cross-field electron mobility in Hall thrusters beyond that provided by collisions with heavy particles. Including these effects can be accomplished by defining the total effective electron collision frequency as

$$\nu_e = \nu_{en} + \nu_{ei} + \nu_w + \nu_b\,, \tag{2}$$

where ν_{en} is the electron-neutral collision frequency, ν_{ei} is the electron-ion collision frequency, ν_w is the collision frequency of the electrons with the lateral walls, and ν_b is a collision frequency defined to capture the effects of turbulent plasma fluctuations.

Determining which of these mechanisms is dominant has been the subject of considerable debate since the 1960s. Experiment, simulation, and theory [13-38] shows that it is likely that both mechanisms each play a role in different regions of the discharge chamber and at different thruster operating conditions. Experimental data from several laboratory Hall thrusters are shown in Figure 1, which plot the plasma potential and Hall parameter, respectively, as a function of axial position from the anode. Position is normalized by the channel length, with the anode at the origin and the exit plane located at z/L=1. Due to the magnetic field distribution, which peaks at the exit plane, the plasma potential must sharply decrease near this maximum in order to maintain current continuity. While turbulence or wall collisionality are often invoked to explain the cross-field transport, the axial variation of the Hall parameter that has been measured is still somewhat surprising. If the mechanism responsible for the anomalous transport could adequately be described simply by invoking Bohm diffusion everywhere, the result would be a slow and gradual decay of the plasma potential across the magnetic field barrier. This is not observed in the structure of the plasma potential and Hall parameter shown in Figure 1, which can be roughly divided in three sections.

In region I, the near-anode region, the Hall parameter is at or below the Bohm value of 16, and approaches the value given by classical collisions alone. The low Hall parameter is driven by the high neutral density that leads to a significant rise in the electron-neutral collision frequency. Plasma simulations support this view [11], which show that the electron-neutral collision frequency dominates in region I, but it is worth pointing out that these simulations typically have significant electric field "leakage" deep in to this region that is not observed experimentally (see Figure 1). While the potential drop found in the simulations is not large, the modeling approach used in this region should not be overlooked since the structure of region I influences the formation of the acceleration region (region II). The electric field perpendicular to the magnetic field in the near-anode region is largely determined by the balance between the resistive and electron-pressure gradient contributions as follows:

$$E_\perp \approx \eta_\perp j_{e,\perp} - \frac{\nabla_\perp p_e}{en}, \quad \eta_\perp = \frac{m_e \nu_e}{e^2 n}\left(1 + \Omega_e^{\,2}\right). \tag{3}$$

Although the Hall parameter is low in this region compared to values observed in region II, it is still high enough that $\Omega_e^{\,2} >> 1$, which implies the following proportionality for the electric field:

$$E_\perp \sim \frac{eB^2}{m_e \nu_e} j_{e,\perp} - \nabla_\perp p_e. \tag{4}$$

We note here that both right-hand-side terms are positive near the anode (z/L<~0.6). Since the electric field observed in the experiment is almost zero here then if the simulations predict a positive value, $E_\perp > 0$, the proportionality above suggests that for a given electron current density distribution the collision frequency is higher than the computed value and/or that the model does not predict accurately the pressure gradient. The first may be due to enhanced collisionality by plasma waves but in view of the small electron-neutral mean free paths it is unlikely that wave growth can be supported in this region. The second is dependent upon the plasma density and electron temperature. The density is mainly driven by the ion motion, which suggests that additional forces on the ions, not presently accounted for in the model, may be leading to a higher density gradient. The behavior of the electron temperature in this region is more difficult to anticipate since it is dependent upon a power balance that is coupled to all of the above. While we will not focus on region I in this paper, we are currently investigating ways to more accurately model this region in our simulations.

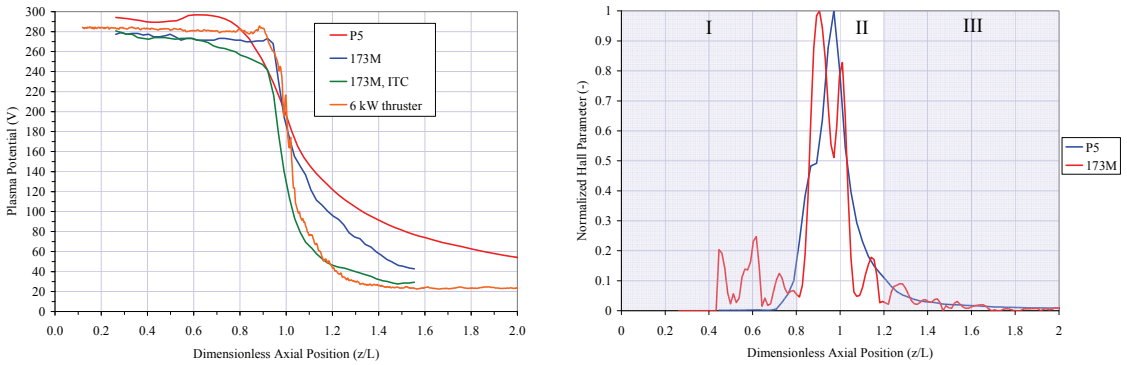

Figure 1. Left: Experimental data showing the axial variation of the plasma potential on the discharge chamber centerline of the P5, NASA-173M, NASA-173M with internal trim coil (ITC), and a 6 kW laboratory thruster. Right: Axial variation of the Hall parameter computed from experimentally measured plasma properties, normalized to its maximum value, on the discharge chamber centerline of the P5 and the NASA-173M. (P5: $\Omega_{e,max}$ = 840, NASA-173M: $\Omega_{e,max}$ = 400). The discharge voltage is 300 V. Position is normalized to the channel length. Data from Ref. [19,27,39].

In region II, the acceleration region, the Hall parameter rapidly increases to a peak value of a few hundred and approaches the value given by classical particle collision alone. The interpretation of this region depends on one's perspective. If one takes the view that the transport should be dictated by

particle collisions alone, then the structure observed in this region indicates that turbulence and wall collisions act to lower the plasma resistivity in order to allow sufficient electron current to pass. Setting aside wall collisionality for the moment, if instead one takes the view that turbulence is present throughout the entire domain, then this region would appear to be one of "turbulence suppression" [40-42]. Cappelli, borrowing from a mechanism that is known to persist in Tokamaks, hypothesized that that the strong axial shear in the ExB drift velocity ($d/dz(E_z/B_r)$) was responsible for the suppression of turbulence in this region. In this view, the strong axial shear tends to stretch and distort turbulent eddies leading to a de-correlation of the eddies that diminishes the turbulent transport. There is a strong level of ExB shear near the exit plane of any modern Hall thruster due to the sharp potential drop that results from the shape of the magnetic field profile. So-called "shear models" of the transport have recently been applied to Hall thrusters because of this. While a firm theoretical basis for this view has yet to be established, the approach may provide a method to predict electron mobility using the value of the ExB shear as a metric, which would eliminate the semi-empirical coefficients that are now used to model the turbulence. Scharfe and Fox [41,42] have implemented different shear models in Hall thruster simulations with encouraging results. However, the effects of the shear models tend to "leak" to far in to regions I and III, leading to higher electric fields and Hall parameters than are experimentally observed. Still, this is an active and emerging area of research that may yet provide a means to predict the mobility in Hall thrusters.

In region III, the near-plume region, the Hall parameter rapidly decays to a value that appears to be far below that of classical theory alone. The reasons for this are unclear. While the presence of turbulence in the region should not be dismissed, it is not immediately clear how strong fluctuations could be driven due to the very low values of the electric field and electron temperature in this region that are measured (see Figure 2) This region is characterized by a decreasing but not insignificant magnetic field, forcing electrons to cross relatively strong field lines in order to enter the discharge chamber. The means by which electrons actually traverse the distance between the cathode and the exit plane are not well established, but interest in this region is increasing [12,38]. Recently, Katz hypothesized that charge exchange collisions in this region could act to transport electrons across the magnetic field in what was termed "ion reflux" [12]. In this view, electrons "hitchhike" on neutrals and when re-ionized in the main beam emerge at a higher potential than where they started. This mechanism, described in detail in Ref [12], could explain why experiments consistently measure such low electron temperatures in this region, while simulations typically have to invoke very high levels of turbulence in order to maintain low potentials and electron temperatures. In our view, these discrepancies are likely driven by an imperfect modeling of this region in the simulations, since, for instance, the present models are not equipped to account for the proposed ion reflux mechanism and are an extension of a physical model that is valid for region II, but begins to lose accuracy in region III (and region I as well). We also demonstrated in Ref. [12] the importance of including doubly-charged ions in the simulation, as they are a significant source of the total current. While Garrigues [43] argued that doubles can be neglected when considering the performance alone, we find that the presence of doubly-charged ions significantly impacts the axial

structure of the current in the thruster and that the neglect of doubles leads to an overestimation of the electron current [12]. There is even evidence that the current fraction of triply-charged xenon is non-negligible, perhaps necessitating yet another ion species in existing simulations [44,45].

In summary, the spatial variation of the Hall parameter in Hall thrusters is a strong function of position. While turbulence is likely the determining factor affecting the electron transport, it is not the sole mechanism acting over the entire domain. The dependencies of the Hall parameter due to classical collisions, wall collisions, turbulence, or other unaccounted for transport mechanisms (e.g., ion reflux, multiply-charged ionization) are imperfectly modeled in existing hybrid-PIC simulations. A focus on turbulence to the neglect of other mechanisms can lead to misleading results when interpreting the plasma response from simulations and must therefore be carefully considered. Due to the imperfect modeling of existing simulations, a variety of approaches have been adopted to describe the variation of the Hall parameter through several semi-empirical coefficients that have less than firm foundations theoretically. New models are emerging and there is considerable experimental and theoretical development underway to understand the cross-field transport, but the existing understanding has not yet provided a predictive capability that captures the physics of the electron transport in Hall thrusters.

Nonetheless, the interest in Hall thrusters for NASA science missions [1,2] requires the development of engineering tools with sufficient fidelity that the plasma magnitudes in the discharge chamber are accurately predicted. At present, these methods require empirical input, but the similarity of the axial dependencies shown in Figure 1 hint that these profiles exhibit a nearly universal dependence. The notion that the Hall parameter profile may be universal, at least in high-efficiency thrusters, was discussed by Hofer and Gallimore [46], where it was also shown that the electron Hall parameter in a high-efficiency Hall thruster averaged 200 over a voltage range of 300-900 V. If the Hall parameter profile is universal, this could provide a means to implement a mobility model that will apply across a broad range of operating conditions and thruster wear. Simulations by Bareilles [47] support this approach, which have shown that maintaining a constant set of parameters over a broad range of operating conditions returned qualitative agreement with experiment data.

Various approaches for describing the anomalous transport are discussed below while details of the other particle and wall collision frequencies are included as an appendix. Anomalous diffusion due to plasma fluctuations is modeled in our simulations as

$$\nu_b = \frac{1}{16}\alpha\omega_{ce}\,, \tag{5}$$

where α is an adjustable parameter that is matched to experiment so that the necessary amount of cross-field diffusion results. In the case of classic Bohm diffusion, α would be equal to one.

Assuming that the functional form for the turbulence provided by Eqn. (5) is appropriate, a predictive model would provide a means to return the value of α as a function of position and time. Barring the availability of a predictive model, the approach in the past has been to ignore temporal dependencies and to crudely discretize the modeling domain in to one or more regions. Based on the experimental data in Figure 1, it seems that the minimum number of regions would be three. However, even for only three

regions there is considerable uncertainty in how to establish the length of each region, how to transition between regions, and the magnitude of the coefficients that are appropriate. The complexity resulting from three-region models has generally been avoided in the literature, with modelers preferring to discretize the domain in to only one or two regions.

In the first version of HPHall, Fife imposed a single value of α over the computational domain [7]. Two-region mobility models have been implemented by Hagelaar and Koo [25,26], and we have implemented our own two-region model in HPHall-2 simulations [4,10,11]. While we have obtained reasonable results, for the reasons described above, it seems clear that the minimum number of regions to be modeled must be at least three. In this paper, we will describe our results from two-region and three-region mobility models. The effects of our choices on the plasma response will be evaluated through comparisons with the plasma properties in the discharge chamber and near-field plume measured in experiments.

In the two-region mobility model, α is defined as

$$\alpha = \begin{cases} \alpha_c & z \le z_c \\ \alpha_c f_c + \alpha_p f_p & z_c < z < z_p \\ \alpha_p & z \ge z_p \end{cases}, \tag{6}$$

where the subscripts c and p refer to channel and plume values, respectively, z is axial position, and the fractions f are defined by

$$\begin{aligned} f_c &= 1 - f_p \\ f_p &= \frac{z - z_c}{z_p - z_c} \end{aligned}. \tag{7}$$

This allows the transition between the channel and plume parameters to vary smoothly over a distance z_p-z_c. The transition between regions is typically chosen to start at the exit plane and to extend downstream by several millimeters.

In the three-region mobility model, α is defined according to

$$\alpha = \begin{cases} \alpha_c & z \le z_c \\ \alpha_c f_c + \alpha_e f_e & z_c < z < z_{e1} \\ \alpha_e & z_{e1} \le z \le z_{e2} \\ \alpha_e f_e + \alpha_p f_p & z_{e2} < z < z_p \\ \alpha_p & z \ge z_p \end{cases}, \tag{8}$$

where the new subscripts *e1* and *e2* refers to the start and end of the region near the exit plane between the channel and plume regions. The fractions for the transition regions are defined similarly to Eqn. (7).

III. Model Updates

A previous article corrected an estimate of the ionization cross-section of singly-charged xenon that had been used since the original version of HPHall [12]. The original cross-section resulted in a significant

underestimation of the current fraction of doubly-charged ions that was not consistent with experiment. It was also recently realized that the inelastic losses due to the creation of doubles were not accounted for in the electron energy equation. This oversight, which dates to the original version of HPHall, might have been due to the low numbers of doubles that were being predicted with the inaccurate ionization cross-section, which would make inelastic losses for doubles also very small. However, with the updated cross-section, we find that the double content is non-negligible and over regions where the double ionization rate peaks, that inelastic losses due to the creation of doubly-charged ions account for more than 10% of the total inelastic losses. To account for these losses, the electron energy equation has been updated as

$$\frac{\partial}{\partial t}\left(\frac{3}{2}n_e k T_e\right) + \nabla\cdot\left(\frac{5}{2}n_e k T_e \vec{u}_e + \vec{q}_e\right) + \dot{E}_w = \vec{j}_e\cdot\vec{E} + S_i\,, \tag{9}$$

where the inelastic loss term accounting for each ionization channel is given by

$$S_i = \left(\dot{n}_i^{+}\varphi E_i\right)^{0\to 1} + \left(\dot{n}_i^{++}E_i\right)^{1\to 2} + \left(\dot{n}_i^{++}E_i\right)^{0\to 2}. \tag{10}$$

Ionization and excitation of the ground state is accounted for in Dugan's ionization cost factor [7,48] given by

$$\varphi\left(T_e/E_i\right) = 2 + 0.254\exp\left(0.677\,E_i/T_e\right), \tag{11}$$

and the excitation of singly- and doubly-charged ions is neglected. Further detail regarding the derivation of the energy equation can be found in Ref. [7,8].

IV. Simulation Inputs and Experimental Results

All plasma simulation results presented here are for a 6 kW laboratory Hall thruster. This thruster is currently being studied at several institutions and serves as a benchmark for studies of basic thruster physics [39,44,45,49-52]. At JPL, the data collected on this thruster are used to validate plasma simulations that are also applied to thrusters being considered for NASA science missions [4]. Experimental data reported in Ref. [39,44,45,49-51] are drawn upon here, as well as previously unreported data from prior experiments at JPL. Details on the experimental configurations can be found in their original source. New data reported here from JPL were collected during the experiments described in Ref. [49,50].

Information on geometry, magnetic field, wall materials, mass flow rate, discharge voltage, etc. are input to the simulation using the known values of the thruster. Grid spacing and time step are chosen to ensure that gradients in the simulation are resolved. The 50x31 grid encompassing the discharge chamber and near-field plume is structured similar to the one shown in Ref. [11]. The axial extent of the simulation and the placement of the cathode boundary condition are chosen such that the ion velocity reaches a constant value. This is done to insure that the entire acceleration region is simulated and that calculations of the thrust are accurate. Simulations were for an operating condition corresponding to a discharge voltage of 300 V and discharge current of 20 A. Thruster characteristics for this operating

condition are given in Table 1. Figure 2 is a near-field mapping of the plume conducted at JPL showing the measured plasma potential and electron temperature. Figure 3 shows axial profiles for the plasma potential, electron temperature, and ion density on the discharge chamber centerline from measurements conducted at the University of Michigan (UM) and JPL. The uncertainty of the measurements are 30% for electron temperature, $0.9*T_e$ for the plasma potential, and 50% for the ion density [39,51]. Agreement between the plasma potential measured at JPL and UM are in good agreement, but the electron temperature near the thruster exit differs by a factor of two. While measurement uncertainty likely contributes to some of the difference, there are known variances between the thruster hardware (each facility has its own thruster) that could have contributed and are presently being investigated further. Throughout this paper, the spatial coordinates are normalized in the axial direction by the channel length (L) and in the radial direction by the mid-diameter of the discharge chamber (D). The anode is located at $z/L = 0$ and the thruster centerline is at $r/D = 0$.

Table 1. Operating conditions and plasma properties for a 6 kW laboratory Hall thruster [39,44,45,49-51]. Data from experiments at JPL unless noted as from the University of Michigan (UM).

Discharge voltage, current	300 V, 20 A			
Anode and cathode mass flow rate	20.98 mg/s, 1.47 mg/s			
Inner and outer coil current	3.51 A, 3.13 A			
Cathode-to-ground voltage	-10 V			
Vacuum chamber pressure	$1.6\text{x}10^{-5}$ torr (JPL), $1.4\text{x}10^{-5}$ torr (UM)			
Ion Energy (plume-averaged)	281 V			
Total Ion Current (from Eqn. (27))	16.3 A			
Ion Current Fractions (plume-averaged) [44]	Xe^+, Xe^{2+}, Xe^{3+} = 0.75, 0.18, 0.07 (UM)			
Plume divergence half-angle (defined as in Ref. [53])	19 degrees (UM)			
Thrust	392-397 mN			
Anode efficiency	61-62%			
Utilization efficiencies (see Appendix for definitions)	Voltage	0.937	Current	0.815
	Divergence	0.897	Mass	0.913
	Charge	0.976		

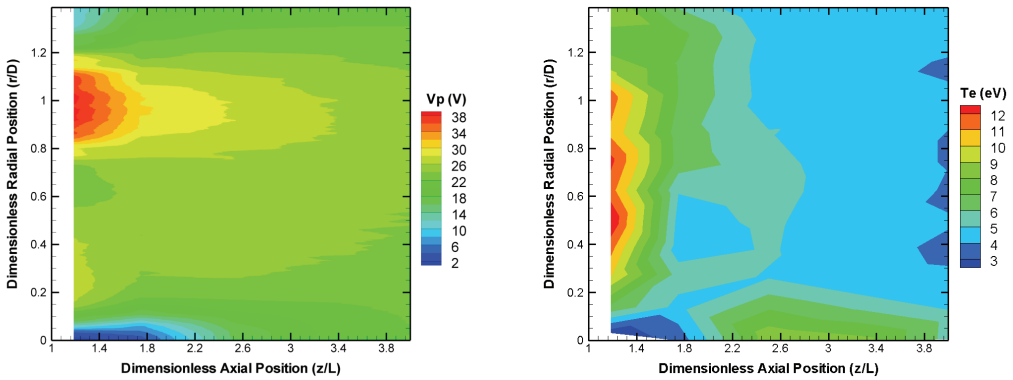

Figure 2. Plasma potential and electron temperature measured in the near-field plume of a 6 kW Hall thruster [49]. The thruster operating conditions are given in Table 1.

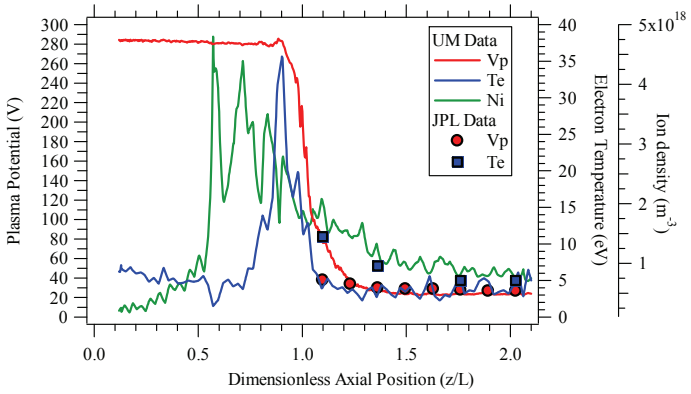

Figure 3. Axial profiles on discharge chamber centerline of the measured plasma potential, electron temperature, and ion density of a 6 kW Hall thruster [39,49]. The thruster operating conditions are given in Table 1.

V. Results

This section presents simulation results for the various electron mobility models that were studied. All simulations were for the thruster operating conditions in Table 1.

A. Two-region mobility model

In the two-region mobility model, optimization of the mobility coefficients is accomplished by setting the plume coefficient α_p to unity and adjusting the channel coefficient α_c so that the experimentally measured discharge current is returned. A channel coefficient of $\alpha_c = 0.044$ was determined to return 20 A discharge current. Thrust and various properties of the discharge current are shown in Table 2. The ion current of 16.5 A is within 1% of the experimentally calculated value of 16.3 A. The thrust of 387 mN is lower than experiment by 1-3%. The Xe^+ current fraction of 0.81 is higher than the plume-averaged value of 0.75 measured in Ref. [44] by 6%.

The various collision frequencies defined in Eqn. (2) and the Hall parameter are shown in Figure 4. The electron-neutral collision frequency dominates near the anode in region I, whereas turbulence

dominates in the plume in region III. In the acceleration zone of region II, it is important to note that turbulence accounts for about half of the total collision frequency, with the balance being due to electron-neutral and wall collisions. The "classical" Hall parameter is also shown in Figure 4 for reference. The classical Hall parameter is the collision frequency given by Eqn. (2) excluding the turbulence collision frequency.

Figure 5 and Figure 6 show the axial variation of the plasma potential, electron temperature, and the various terms of the energy equation defined in Eqn. (9) on the centerline of the discharge chamber. Comparisons to experiment are shown in Figure 5. Recalling that the uncertainty of the electron temperature and plasma potential are 30% and 0.9*T_e, respectively, the agreement between simulation and experiment is fair over most of the domain. The plasma potential qualitatively agrees with the experiment, but has significantly lower slope in the acceleration region and significantly higher slope in the plume. The electron temperature agrees well with experiment in region I and II, but is much higher in the plume. The power balance shown in Figure 6 shows that the electron temperature is determined primarily by the competing effects of Ohmic heating due to the electric field, electron wall losses, and inelastic losses due to ionization. The Ohmic heating term is non-negligible over the entire domain, but this is in poor agreement with experiment. Low Ohmic heating in regions I and III can be inferred from the experimental data in Figure 2 and Figure 5, which show nearly negligible gradients in the potential and electron temperature.

In summary, the two-region mobility model can accurately predict the thrust and discharge current, but has shortcomings with respect to the spatial distribution of the plasma potential and electron temperature. These deficiencies likely affect the accuracy of any hybrid-PIC simulation that makes use of the two-region model [25,26,30] and has implications for erosion modeling, which is sensitive to the distribution of the plasma magnitudes in the discharge chamber [4].

Table 2. Simulation results using the two-region mobility model. ($\alpha_c = 0.044$, $\alpha_p = 1.0$, $p = 0$ torr)

Thrust (mN) =	387
Discharge Current (A) =	20
Ion Current (A) =	16.5
Xe^+ Current Fraction (-) =	0.81
Xe^{2+} Current Fraction (-) =	0.19

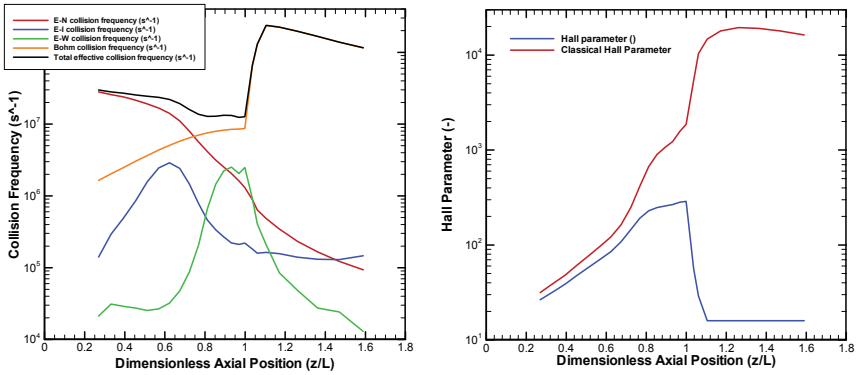

Figure 4. Collision frequency and Hall parameter versus axial position from simulations using the two-region mobility model. Values are volume weighted averages over magnetic field lines. ($\alpha_c = 0.044$, $\alpha_p = 1.0$, $p = 0$ torr)

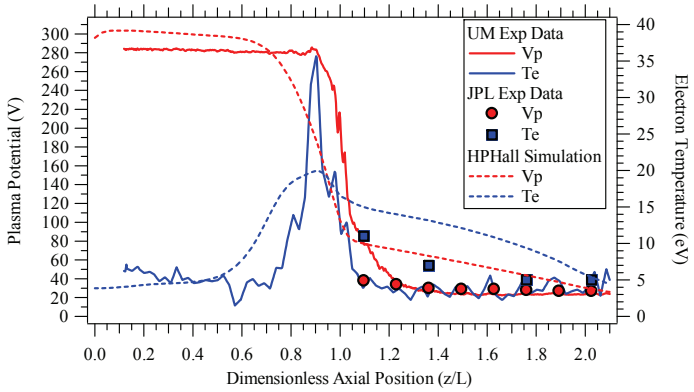

Figure 5. Plasma potential and electron temperature from experiment and simulations using the two-region mobility model. Values are taken on discharge chamber centerline. ($\alpha_c = 0.044$, $\alpha_p = 1.0$, $p = 0$ torr)

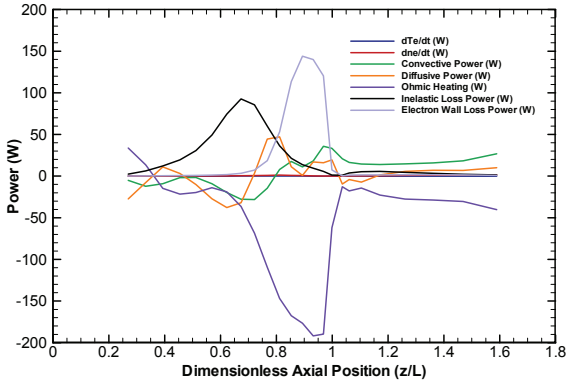

Figure 6. Energy equation terms versus axial position from simulations using the two-region mobility model. Values are volume weighted averages over magnetic field lines. ($\alpha_c = 0.044$, $\alpha_p = 1.0$, $p = 0$ torr)

B. Three-region mobility model

1. Baseline Results

In the three-region mobility model, optimization of the mobility coefficients is accomplished by setting the plume coefficient α_p to unity and adjusting the channel and exit coefficients (α_c and α_e) so that the experimentally measured discharge current is returned. A channel coefficient of $\alpha_c = 0.14$ and an exit coefficient of $\alpha_e = 0.02$ were determined to return 20.2 A discharge current (time constraints prohibited a more precise matching to 20 A).

Various properties of the simulation are shown in Table 3 and Figure 7 through Figure 9. Overall, the simulation yields properties that are more consistent with experiment than the two-region model. The ion current of 16.3 A matches the experiment, yet the thrust still lags at 386 mN. Gradients in the plasma potential are increased, as expected, due to the sharp decrease in mobility through the acceleration zone in region II. While there is still "leakage" in regions I and III, the profiles of the Ohmic heating and wall loss terms are significantly less broad than the profiles from the two-region model. The electron-neutral, wall, and turbulence collision frequencies are all within roughly a factor of five in region II. While evident that turbulence is necessary to account for the electron transport, it is far from being the sole determining factor in region II. In the next few sections, we will explore several numerical experiments that were performed to examine how the agreement between the simulation and experiment for the electron temperature and plasma potential can be improved.

Table 3. Simulation results using the three-region mobility model. ($\alpha_c = 0.14$, $\alpha_e = 0.02$, $\alpha_p = 1.0$, $p = 0$ torr)

Thrust (mN) =	386
Discharge Current (A) =	20.2
Ion Current (A) =	16.3
Xe^+ Current Fraction (-) =	0.83
Xe^{2+} Current Fraction (-) =	0.17

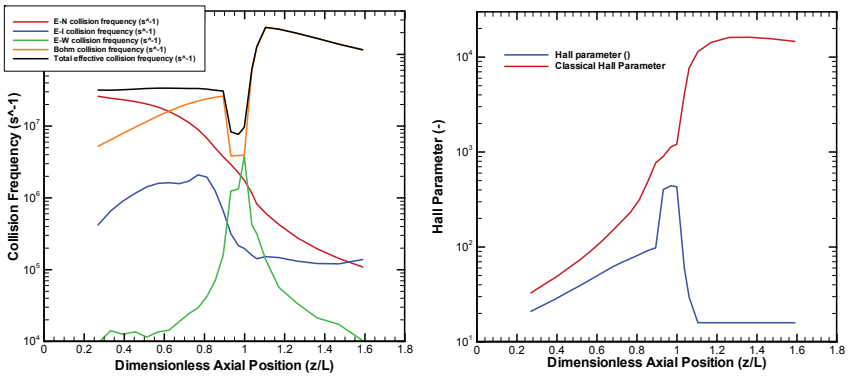

Figure 7. Collision frequency and Hall parameter versus axial position from simulations using the three-region mobility model. Values are volume weighted averages over magnetic field lines. ($\alpha_c = 0.14$, $\alpha_e = 0.02$, $\alpha_p = 1.0$, $p = 0$ torr)

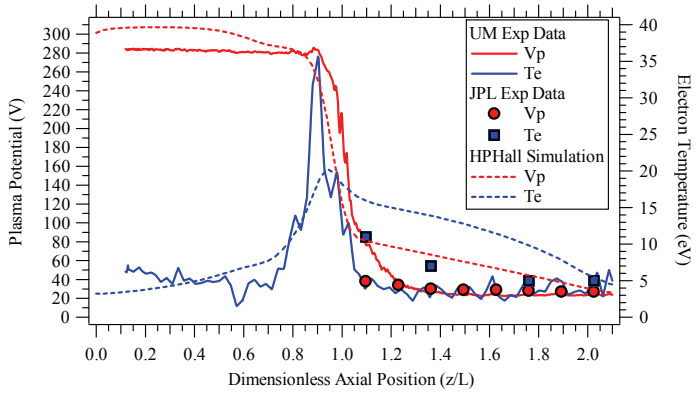

Figure 8. Plasma potential and electron temperature from experiment and simulations using the three-region mobility model. Values are taken on discharge chamber centerline. ($\alpha_c = 0.14$, $\alpha_e = 0.02$, $\alpha_p = 1.0$, $p = 0$ torr)

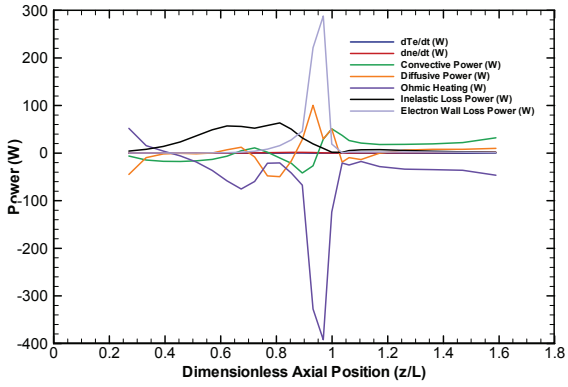

Figure 9. Energy equation terms versus axial position from simulations using the three-region mobility model. Values are volume weighted averages over field lines. ($\alpha_c = 0.14$, $\alpha_e = 0.02$, $\alpha_p = 1.0$, $p = 0$ torr)

2. Structure of the near-field plume (Region II)

Both the two- and three-region mobility models show gradients in the plasma potential and electron temperature in the near-field plume that are not measured experimentally. This is despite the fact that both models impose plume coefficients for the turbulence of 1.0, that is, the Hall parameter is set to the Bohm value of 16. The poor agreement should not be surprising however if one considers the Hall parameter computed from measured plasma properties. Figure 10 shows the axial profile of the Hall parameter starting at the discharge chamber exit plane from the P5 and NASA-173M. (The Hall parameter of the 6 kW thruster have not yet been computed, but the same trend is expected.) The Hall parameter falls below the Bohm value of 16 between z/L=1.2-1.5 and goes to just $1/10^{th}$ of the Bohm value (~2) by z/L= 1.7. Assuming for a moment that turbulence is solely responsible for the decay in the Hall parameter, this implies a plume coefficient for the turbulence that is ten times the Bohm value.

The source of this strong decay of the Hall parameter could be through turbulence or other mechanisms that are not accounted for in the code such as ion reflux. Simulations were conducted to test how the near-field plume structure is affected by changes to the simulation parameters. These simulations included: a) setting the turbulence plume coefficient to 10, and b) activating the vacuum facility backpressure model so that a higher neutral density would persist in the near-field plume. Results from each of these simulations are discussed below.

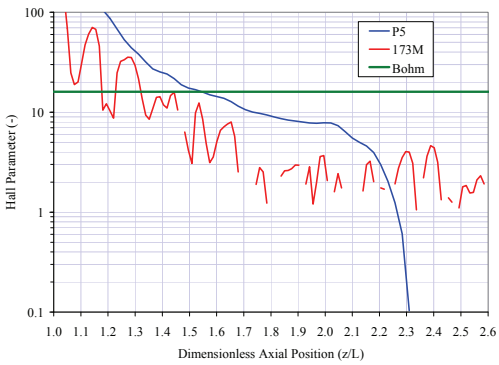

Figure 10. Axial variation of the Hall parameter on the discharge chamber centerline of the P5 and the NASA-173M for a discharge voltage of 300 V. The Hall parameter falls below the Bohm value of 16 between z/L=1.2-1.5 and goes to $1/10^{th}$ of the Bohm value (~2) by z/L= 1.7. Data from Ref. [19,27].

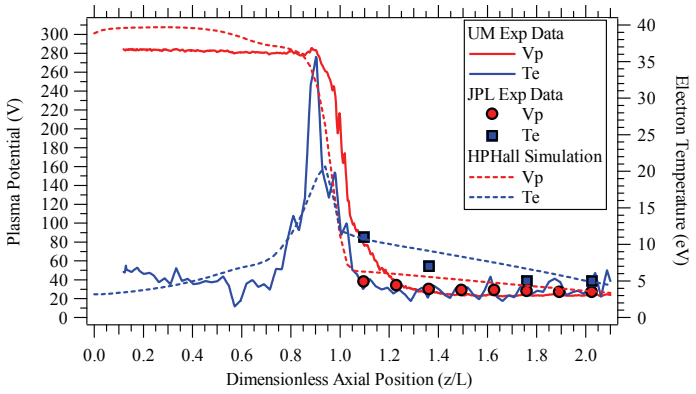

Figure 11. Plasma potential and electron temperature from experiment and simulation using the three-region mobility model with $\alpha_p = 10$ in the plume. Values are taken on discharge chamber centerline. ($\alpha_c = 0.14$, $\alpha_e = 0.02$, $\alpha_p = 10.0$, $p = 0$ torr)

Figure 11 shows the electron temperature and plasma potential profiles when the turbulence coefficient in the plume is set to 10. These settings are very effective at suppressing electric fields and electron heating in the plume and the agreement with experiment is significantly improved. Although a plume coefficient of 10 results in excellent agreement with experiment, we emphasize that transport in the plume is not necessarily the result of turbulence and could be due to other mechanisms that are not accounted for in the code presently [12,38].

Collisions in the near-field plume with background neutrals could be a source of transport that is not adequately modeled in the code. Our simulations typically do not include background neutrals, but there is an option in HPHall to include a background pressure to simulate vacuum facility effects. To examine the effects of a finite background of neutrals, numerical experiments were first conducted using the measured backpressure of 1.6×10^{-5} torr. The results were almost unchanged from the vacuum conditions. However, if the backpressure is raised to ten times the measured value, there is a significant change in the plume structure. This is shown in Figure 12, which shows that the electric field and electron temperature are much reduced in the plume. Although the simulation required a backpressure ten times the measured value, it is still surprising that the potential structure could be affected this strongly simply due to the presence of neutrals. If there were a mechanism, such as ion reflux [12], that would effectively raise the neutral density in the near-field plume, then the net effect could be very similar to what is observed in our simulations. It should also not go unnoticed that the high-pressure model is nearly equivalent to imposing high-mobility in the plume. Neither of these approaches definitively identify the source of the anomalous mobility in the plume, but they do illustrate that classical effects could contribute to the mobility and that turbulence should not be assumed *à priori*. Models that could account for mechanisms such as ion reflux are presently being considered.

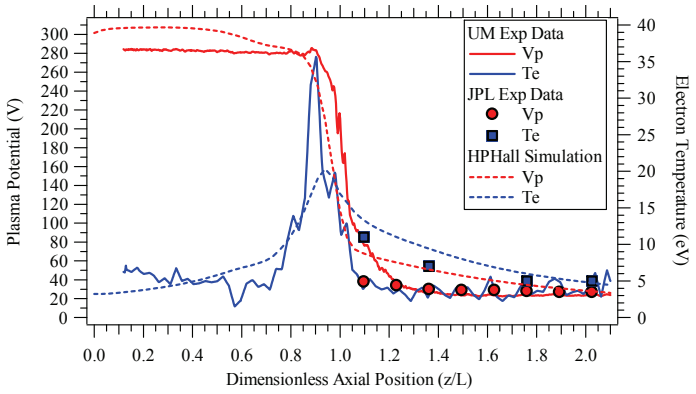

Figure 12. Plasma potential and electron temperature from experiment and simulation using the three-region mobility model with a backpressure of 1x10^{-4} torr (10X measured). Values are taken on discharge chamber centerline. ($\alpha_c = 0.14$, $\alpha_e = 0.02$, $\alpha_p = 1.0$, $p = 1\text{x}10^{-4}$ torr)

3. Electron temperature anisotropy

Regardless of the electron mobility model used, the simulations return maximum electron temperatures of about 20 eV, which under predicts the experiment by 5-10 eV. While this is still within the 30% uncertainty of the data [51], thrust is generally under predicted by 1-3%. The differences could be due to the assumptions in the code of isotropic electron temperature and 100% thermalization of the secondary electrons emitted from the wall. The sheath model also does not treat the population of secondaries emitted from the wall as a separate species. Rather, it assumes that secondary electrons completely thermalize with the bulk plasma at the sheath edge. Due to these assumptions, any depletion of the high-energy tail in the direction parallel to the magnetic field lines is not captured. This depletion occurs due to the loss of electrons to the wall with sufficient energy to overcome the wall sheath potential. Kinetic simulations have shown that the temperature of electrons parallel and perpendicular to the magnetic field lines are not equal and have attributed this anisotropy for the reasons stated above [31].

As a crude way to model anisotropy of the electron temperature, the temperature of electrons impacting the wall was reduced by a fixed ratio. Doing so reduces the wall energy losses, resulting in higher electron temperatures, ionization rates, and thrust. In Figure 13, the electron temperature increases by about 5 eV to a maximum of 25 eV for a three-region mobility model with a temperature ratio of $T_{e\|}/T_{e\perp} = 0.86$. Thrust also increased to 395 mN, which is in excellent agreement with experiment. Future work on this approach will consider other self-consistent methods to account for anisotropy of the electron temperature and the wall sheath model that is used, possibly by accounting for partial thermalization or sheath models derived from kinetic simulations [31,54].

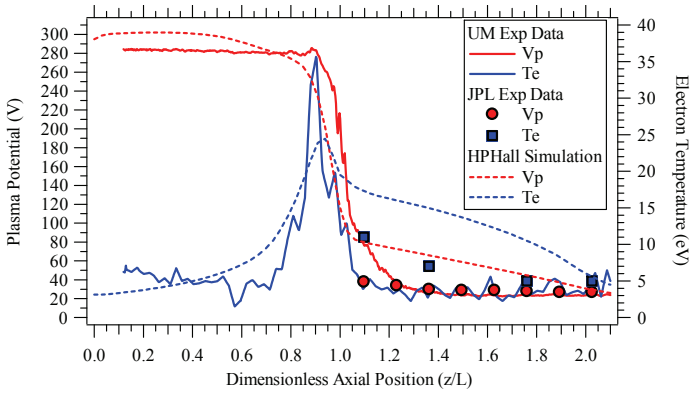

Figure 13. Plasma potential and electron temperature from experiment and simulation using the three-region mobility model with anisotropic electrons ($T_{e||}/T_{e\perp} = 0.86$). The anisotropy raises the maximum electron temperature to approximately 25 eV and the thrust to 395 mN (not shown). Values are taken on discharge chamber centerline. ($\alpha_c = 0.08$, $\alpha_e = 0.02$, $\alpha_p = 1.0$, $p = 0$ torr)

VI. Discussion

A. Evaluation of the various mobility models

The various simulations described above have examined the effects of the electron mobility on the macro- and microscopic properties returned from a hybrid-PIC simulation of the Hall thruster. Several models of varying complexity were considered:

1. Two-region mobility
2. Three-region mobility
3. High-mobility in the plume
4. High-pressure in the plume
5. Anisotropic electrons

The two-region mobility model that has been used in our previous work is shown to inadequately describe the distribution of plasma magnitudes in the discharge chamber. While this model can accurately reproduce macroscopic properties such as the thrust and ion current, the microscopic properties are not predicted nearly as well. This would likely impact negatively the accuracy of erosion calculations, the ultimate goal of this work, as predicting the wear of the discharge chamber walls over thousands of hour of operation at different operating conditions is affected by the distribution of plasma potential and electron temperature in the channel.

The three-region mobility model is a significant improvement over the two-region model, as there is considerably improved agreement of the structure of the acceleration region. However, electric field leakage in region I and region III are still present, motivating an examination of how the mobility model needed to be modified in order to better reproduce experimental results.

In the plume (region III), experiments suggest that the Hall parameter is actually quite low, on the order of 2 ($1/10^{\text{th}}$ the Bohm value). This fact seems to have been overlooked in the literature and

deserves significantly more scrutiny. When we apply high-mobility or high-pressure in the plume, we find that both approaches are very effective at maintaining the electron temperature and plasma potential to levels that are measured experimentally. While these simulations do not offer an explanation of the underlying physics, they do serve to highlight that existing hybrid-PIC models must be modified to more accurately reflect the physics of this region. For the sake of computational expediency, since the high-pressure option requires a large increase of the neutrals in the simulation, we have chosen to move forward using the high-mobility option in the simulation. Models that could account for other transport mechanisms such as ion reflux [12] are presently being considered.

The simple model explored here to consider the impact of anisotropy in the electron velocity distribution function has yielded positive results. By adjusting the ratio of the parallel to perpendicular electron temperature, we can control the wall losses and predict more accurate magnitudes of the ion current and thrust. Future work though needs to formally address how to modify the sheath models used in the code, perhaps by accounting for partial thermalization of the electrons or sheath models derived from kinetic simulations [31,54].

In summary, we find the best agreement with experiment when the three-region mobility model is applied using high-mobility in the plume and anisotropic electrons. Results from a simulation implementing this combined model are discussed below.

B. Plasma properties using the final mobility model

A final simulation incorporating aspects of the various models that most accurately reproduce the experimental data is presented in this section. This simulation made use of the three-region mobility model with temperature anisotropy and high mobility in the plume, corresponding to: ($\alpha_c = 0.065$, $\alpha_e = 0.02$, $\alpha_p = 10$, p = 0 torr, $T_{e||}/T_{e\perp} = 0.86$). Table 4 shows the global properties of the simulation are in excellent agreement with experiment, yielding thrust of 393 mN and ion current of 16.4 A. Collision frequency, Hall parameter, plasma potential, electron temperature, plasma density and the terms of the energy equation are shown in Figure 14 through Figure 17. The profiles of electron temperature, plasma potential, and plasma density are in good agreement overall with experiment, displaying similar qualitative and quantitative properties. Recalling that the uncertainty of the measurements are 30% for electron temperature, 0.9*T_e for the plasma potential, and 50% for the ion density [39,51], the differences shown in the figures are within this uncertainty over the majority of the simulation domain. One notable exception is the potential gradient, which is well reproduced except for its axial location, a difference that can be improved on by adjusting the location of region II in the mobility model. Overall, the simulation is successful at reproducing global properties such as thrust and detailed distributions of the plasma magnitudes in the discharge chamber.

Table 4. Simulation results using the three-region mobility model with anisotropic electrons and high mobility in the plume. ($\alpha_c = 0.065$, $\alpha_e = 0.02$, $\alpha_p = 10$, $p = 0$ torr, $T_{e||}/T_{e\perp} = 0.86$)

Thrust (mN) =	393
Discharge Current (A) =	20.0
Ion Current (A) =	16.4
Xe^+ Current Fraction (-) =	0.81
Xe^{2+} Current Fraction (-) =	0.19

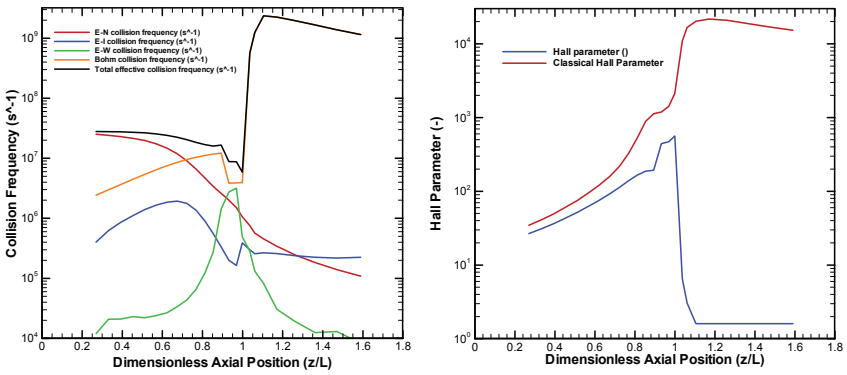

Figure 14. Collision frequency and Hall parameter versus axial position from simulations using the three-region mobility model with anisotropic electrons and high mobility in the plume. Values are volume weighted averages over magnetic field lines. ($\alpha_c = 0.065$, $\alpha_e = 0.02$, $\alpha_p = 10$, $p = 0$ torr, $T_{e||}/T_{e\perp} = 0.86$)

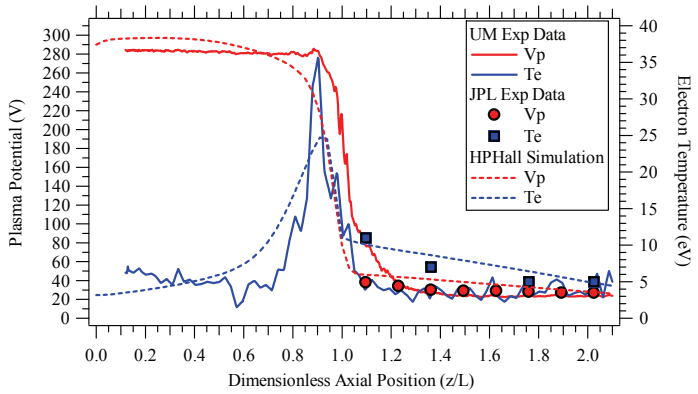

Figure 15. Plasma potential and electron temperature from experiment and simulations using the three-region mobility model with anisotropic electrons and high mobility in the plume. Values are taken on discharge chamber centerline. ($\alpha_c = 0.065$, $\alpha_e = 0.02$, $\alpha_p = 10$, $p = 0$ torr, $T_{e||}/T_{e\perp} = 0.86$)

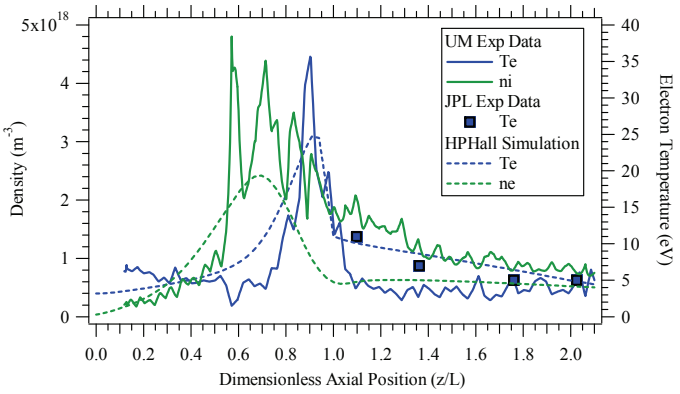

Figure 16. Plasma density and electron temperature from experiment and simulations using the three-region mobility model with anisotropic electrons and high mobility in the plume. Values are taken on discharge chamber centerline. ($\alpha_c = 0.065$, $\alpha_e = 0.02$, $\alpha_p = 10$, $p = 0$ torr, $T_{e||}/T_{e\perp} = 0.86$)

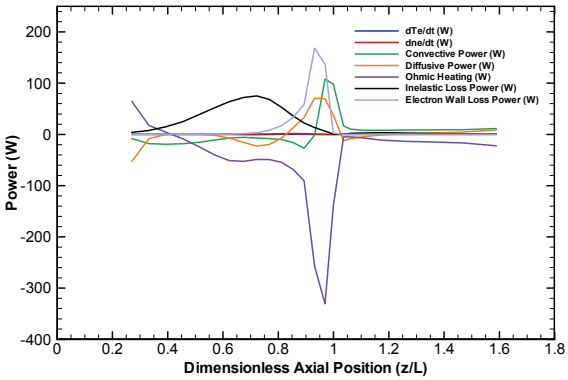

Figure 17. Energy equation terms versus axial position from simulations using the three-region mobility model with anisotropic electrons and high mobility in the plume. Values are volume weighted averages over field lines. ($\alpha_c = 0.065$, $\alpha_e = 0.02$, $\alpha_p = 10$, $p = 0$ torr, $T_{e||}/T_{e\perp} = 0.86$)

VII. Conclusion

Experimental data of the plasma properties inside Hall thrusters reveals a complex dependence along the axial extent of the discharge chamber. Two-region mobility models that have been extensively reported in the literature are incapable of capturing the large gradients in the electron Hall parameter that have been measured in multiple thrusters. Parametric studies of alternate mobility models in this work have considered a three-region model, the effects of high-mobility and high-pressure in the plume, and electron temperature anisotropy. The three-region model substantially improved the agreement of the plasma potential and electron temperature profiles with experiment. A high level of mobility in the plume was required to reproduce plasma potential consistent with measurements. The results found after invoking high-pressure in the plume suggest that other mechanisms not currently modeled may be present that effectively enhance the electron transport in the near-plume. The simple model for temperature

anisotropy needs to be formally implemented through a reconsideration of the sheath model. It was found that the simulation most consistent with experiment was the three-region model using temperature anisotropy and high plume mobility.

While the models used here do not provide an explanation for anomalous transport, the insight gained through careful comparisons of the simulations with experimental data provides a guide to future theoretical studies of electron mobility in Hall thrusters. The axial variation of the Hall parameter is extremely complex and is poorly modeled with simple two-region mobility models. Although the three-region model does not provide a predictive capability, we emphasize that this model has been shown to reproduce the experimentally measured plasma properties quite well and should therefore provide higher fidelity results of the plasma properties and wall erosion.

Future work will focus on testing the robustness of the three-region mobility model across multiple operating conditions and thruster life. Even if the three-region model proves to have limited predictive capability, it is certainly possible to measure the internal properties of thrusters being considered for long duration missions so that erosion models can be adequately calibrated. Measurements of this type were extremely rare until the 1990s, but have now become almost routine at several institutions in the United States. The goal of a fully-predictive model is likely some way off, but the research being conducted in this area of Hall thruster physics may yet produce predictive models.

Acknowledgements

The research described in this paper was carried out at the Jet Propulsion Laboratory, California Institute of Technology, under a contract with the National Aeronautics and Space Administration.

We would also like to thank James Haas, Jesse Linnell, Bryan Reid, and Alec Gallimore for sharing their plasma measurements.

Appendix – Particle and Wall Collisions

The electron mobility model described in the main text accounts for the cross-field electron transport due to plasma turbulence and collisions with neutrals, ions, and walls. Models describing the turbulence are described in the main text. This section presents details on how the remaining collision frequencies are modeled.

The electron-neutral collision frequency is modeled as

$$\nu_{en} = n_n Q_{en} \sqrt{\frac{8kT_e}{\pi m_e}}\,, \tag{12}$$

where Q_{en} is the Maxwellian averaged cross-section of McEachran and Stauffer [55] described by an analytical fit given by

$$Q_{en} = \begin{cases} 7.55 \times 10^{-20} & T_e < 1\ eV \\ 10^{-20}\left(\dfrac{94\left(\dfrac{T_e}{2.21} \text{-} 0.364 \right)}{\left(1 + \left(\dfrac{T_e}{2.21} \right)^{1.7} \right)} + \dfrac{18\,T_e}{18 + T_e} \right) & T_e \geq 1\ eV \end{cases}, \tag{13}$$

where T_e is the electron temperature in eV and $Q_{e\text{-}n}$ is in m^2.

The electron-ion collision frequency is modeled as [56]

$$\nu_{ei} = 2.91 \times 10^{-12} n_e T_e^{-3/2} \ln \Lambda\ , \tag{14}$$

with the electron temperature in eV and the Coulomb logarithm given by

$$\ln \Lambda = \begin{cases} 23 - \log\left(T_e^{-3/2} \sqrt{10^{-6} n_e} \right) & T_e \leq 10\ \text{eV} \\ 24 - \log\left(T_e^{-1} \sqrt{10^{-6} n_e} \right) & T_e > 10\ \text{eV} \end{cases}. \tag{15}$$

The wall collision frequency is modeled as

$$\nu_w(\ell,\chi) = \frac{\left(\left[\Delta A \dfrac{\delta_w}{1-\delta_w} \Gamma_{brQ} \right]_{IW} + \left[\Delta A \dfrac{\delta_w}{1-\delta_w} \Gamma_{brQ} \right]_{OW} \right)}{\Delta V(\ell)\, n_e(\ell,\chi)}, \tag{16}$$

where ℓ =1,2,…,n is the magnetic field line index, χ is the coordinate along the magnetic field line, ΔA and ΔV are area and volume elements centered on the magnetic field line, the subscripts IW and OW refer to the inner and outer wall, and the rest of the symbols are defined in the Nomenclature section.

Appendix - Phenomenological Model of Hall Thruster Performance

We complete the phenomenological Hall thruster performance model presented in Ref. [57] by explicitly including the plume divergence. In Ref. [57], plume divergence was included as part of the voltage utilization efficiency, but overestimated this quantity because the results were derived from thruster centerline measurements of the ion energy (the effects of divergence were actually included as additional negative uncertainty in the voltage utilization). The model here expresses the performance of a Hall thruster as a function of the utilization efficiencies of current, mass, voltage, divergence, and charge by accounting for a partially-ionized, multiply-charged plasma. When combined with experimental data, the model can be used to weigh the relative importance of various plasma properties affecting performance such as multiply-charged ions or the electron current.

Excluding the electrical efficiency of the systems that deliver power to a Hall thruster, the total thrust efficiency (η_t) is the ratio of jet power in the exhaust to the total input power

$$\eta_t = \frac{P_{jet}}{P_t} = \frac{T^2}{2\dot{m}_a P_d} \frac{P_d}{P_t} \frac{\dot{m}_a}{\dot{m}_t} = \eta_a \eta_{mag} \eta_c\,. \tag{17}$$

The cathode efficiency (η_c) and electromagnet efficiency (η_{mag}) account for the cathode flow rate and the power supplied to the electromagnet coils, respectively. Since these losses are not directly related to the production of useful thrust, the focus here is on the anode efficiency (η_a).

The anode efficiency is determined by the efficiency of the ionization and acceleration processes. While these processes are interrelated and not easily separated analytically, one way to decompose the anode efficiency is by defining the following utilization efficiencies:

1. *charge utilization efficiency:* the net efficiency decrease due to multiply-charged ions;
2. *voltage utilization efficiency:* the conversion of voltage into axially directed ion velocity;
3. *plume divergence utilization efficiency:* the loss of axially-directed momentum due to the divergence of the ion beam;
4. *current utilization efficiency:* the fraction of ion current contained in the discharge current; and
5. *mass utilization efficiency:* the conversion of neutral mass flux into ion mass flux.

Following the methodology described in Ref. [57] and adding a term to explicitly account for the plume divergence, the thrust can be expressed as

$$T = \sum \dot{m}_i \langle v_i \rangle = \eta_b I_d \sqrt{\frac{2 m_{xe} \eta_v V_d}{e}} \sum \frac{\Omega_i}{\sqrt{Z_i}} \cos\theta \,, \tag{18}$$

where the summation is for each ion species i from 1 to N, where N is the total number of ion species. The anode specific impulse can be expressed as,

$$I_{sp,a} = \frac{T}{\dot{m}_a g} = \frac{\eta_m}{g} \sqrt{\frac{2 e \eta_v V_d}{m_{xe}}} \frac{\sum \frac{\Omega_i}{\sqrt{Z_i}}}{\sum \frac{\Omega_i}{Z_i}} \cos\theta \,, \tag{19}$$

and the anode efficiency is the product of the five utilization efficiencies given by

$$\eta_a = \frac{T^2}{2 \dot{m}_a P_d} = \eta_q \eta_v \eta_d \eta_b \eta_m \,. \tag{20}$$

The partial efficiencies are the charge utilization efficiency

$$\eta_q = \frac{\left(\sum \Omega_i / \sqrt{Z_i} \right)^2}{\sum \Omega_i / Z_i} \,, \tag{21}$$

the voltage utilization efficiency

$$\eta_v = \frac{V_a}{V_d} = 1 - \frac{V_l}{V_d}, \tag{22}$$

the divergence utilization efficiency

$$\eta_d = \left(\cos\theta\right)^2, \tag{23}$$

the current utilization efficiency

$$\eta_b = \frac{I_b}{I_d} = 1 - \varepsilon, \tag{24}$$

and the mass utilization efficiency

$$\eta_m = \frac{\dot{m}_b}{\dot{m}_a} = \xi\eta_b \sum \frac{\Omega_i}{Z_i}. \tag{25}$$

In the above, the plume divergence angle is defined according to [58]

$$\cos\theta = \frac{\int_0^{2\pi}\int_{R_i}^{R_o} j_{bz} r dr d\phi}{\int_0^{2\pi}\int_{R_i}^{R_o} \left|\vec{j}_b\right| r dr d\phi} = \frac{\int_{R_i}^{R_o} j_{bz} r dr}{\int_{R_i}^{R_o} \left|\vec{j}_b\right| r dr}, \tag{26}$$

where the limits of integration, R_i and R_o, are appropriate limits capturing the ion beam, j_z is the axial component of the ion current density, and $\vec{j}$ is the ion current density vector. In simulations, the integration plane is chosen at an axial location near the edge of the computational boundary.

The current, mass, and charge utilization efficiencies are interrelated due to their dependence on the ion current and the ion current fractions. Thus, the anode efficiency can also be expressed as

$$\eta_a = \eta_d \eta_v \underbrace{\left(1-\varepsilon\right)^2 \xi \left(\sum \frac{\Omega_i}{\sqrt{Z_i}}\right)^2}_{\eta_b \eta_m \eta_q}. \tag{27}$$

The electron current fraction (ε) can be calculated using Eqn. (27) if the anode efficiency, plume divergence angle, ion current fractions, and ion loss voltage are known. Equations (21) through (25) can then be used to compute each of the utilization efficiencies. Typically, anode efficiency is computed from thrust measured with a thrust stand, plume divergence is measured with a Faraday probe, the ion current fractions are measured with an ExB probe, and the ion loss voltage is measured with a retarding potential analyzer. Whenever possible, plume-averaged quantities for the ion current fractions and ion loss voltage

should be used, although there are situations where measurements on thruster centerline may be sufficient to accurately characterize these quantities [44].

References

[1] Hofer, R. R., Randolph, T. M., Oh, D. Y., Snyder, J. S., and de Grys, K. H., "Evaluation of a 4.5 kW Commercial Hall Thruster System for NASA Science Missions," AIAA Paper 2006-4469, July 2006.

[2] Randolph, T. M., "Qualification of Commercial Electric Propulsion Systems for Deep Space Missions," Presented at the 30th International Propulsion Conference, IEPC Paper 2007-271, Florence, Italy, Sept. 17-20, 2007.

[3] Katz, I., Mikellides, I. G., Wirz, R., Anderson, J. R., and Goebel, D. M., "Ion Thruster Life Models," AIAA Paper 2005-4256, July 2005.

[4] Hofer, R. R., Mikellides, I. G., Katz, I., and Goebel, D. M., "BPT-4000 Hall Thruster Discharge Chamber Erosion Model Comparison with Qualification Life Test Data," Presented at the 30th International Electric Propulsion Conference, IEPC Paper 2007-267, Florence, Italy, Sept. 17-20, 2007.

[5] Mikellides, I. G. and Katz, I., "Wear Mechanisms in Electron Sources for Ion Propulsion, 1: Neutralizer Hollow Cathode," Journal of Propulsion and Power 24, 4, 855 (2008).

[6] Mikellides, I. G., Katz, I., Goebel, D. M., Jameson, K. K., and Polk, J. E., "Wear Mechanisms in Electron Sources for Ion Propulsion, 2: Discharge Hollow Cathode," Journal of Propulsion and Power 24, 4, 866 (2008).

[7] Fife, J. M., "Hybrid-PIC Modeling and Electrostatic Probe Survey of Hall Thrusters," Ph.D. Thesis, Aeronautics and Astronautics, Massachusetts Institute of Technology, 1998.

[8] Parra, F. I., Ahedo, E., Fife, J. M., and Martinez-Sanchez, M., "A Two-Dimensional Hybrid Model of the Hall Thruster Discharge," Journal of Applied Physics 100, 023304 (2006).

[9] Gamero-Castano, M. and Katz, I., "Estimation of Hall Thruster Erosion Using HPHall," Presented at the 29th International Electric Propulsion Conference, IEPC Paper 2005-303, Princeton, NJ, Oct. 31-Nov. 4, 2005.

[10] Hofer, R. R., Katz, I., Mikellides, I. G., and Gamero-Castano, M., "Heavy Particle Velocity and Electron Mobility Modeling in Hybrid-PIC Hall Thruster Simulations," AIAA Paper 2006-4658, July 2006.

[11] Hofer, R. R., Mikellides, I. G., Katz, I., and Goebel, D. M., "Wall Sheath and Electron Mobility Modeling in Hybrid-PIC Hall Thruster Simulations," AIAA Paper 2007-5267, July 2007.

[12] Katz, I., Hofer, R. R., and Goebel, D. M., "Ion Current in Hall Thrusters," IEEE Transactions on Plasma Science (accepted for publication, 2008).

[13] Janes, G. S. and Lowder, R. S., "Anomalous Electron Diffusion and Ion Acceleration in a Low-Density Plasma," Physics of Fluids 9, 6 (1966).

[14] Morosov, A. I., Esipchuk, Y. V., Tilinin, G. N., Trofimov, A. V., Sharov, Y. A. et al., "Plasma Accelerator with Closed Electron Drift and Extended Acceleration Zone," Soviet Physics Technical Physics 17, 1 (1972).

[15] Esipchuk, Y. B., Morosov, A. I., Tilinin, G. N., and Trofimov, A. V., "Plasma Oscillations in Closed-Drift Accelerators with an Extended Acceleration Zone," Soviet Physics - Technical Physics 18, 7 (1974).

[16] Esipchuk, Y. V. and Tilinin, G. N., "Drift Instability in a Hall-Current Plasma Accelerator," Soviet Physics - Technical Physics 21, 4, 417-429 (1976).

[17] Tilinin, G. N., "High-Frequency Plasma Waves in a Hall Accelerator with an Extended Acceleration Zone," Soviet Physics - Technical Physics 22, 8, 974-978 (1977).

[18] Bishaev, A. M. and Kim, V., "Local Plasma Properties in a Hall-Current Accelerator with an Extended Acceleration Zone," Soviet Physics Technical Physics 23, 9 (1978).

[19] Haas, J. M., "Low-Perturbation Interrogation of the Internal and near-Field Plasma Structure of a Hall Thruster Using a High-Speed Probe Positioning System," Ph.D. Dissertation, Aerospace Engineering, University of Michigan, 2001.

[20] Gascon, N., Dudeck, M., and Barral, S., "Wall Material Effects in Stationary Plasma Thrusters I: Parametric Studies of an SPT-100," Physics of Plasmas 10, 10, 4123-4136 (2003).

[21] Barral, S., Makowski, K., Peradzynski, Z., Gascon, N., and Dudeck, M., "Wall Material Effects in Stationary Plasma Thrusters II: Near-Wall and in-Wall Conductivity," Physics of Plasmas 10, 10, 4137-4152 (2003).

[22] Choueiri, E. Y., "Plasma Oscillations in Hall Thrusters," Physics of Plasmas 8, 4, 1411-1426 (2001).

[23] Meezan, N. B., Hargus, W. A., and Cappelli, M. A., "Anomalous Electron Mobility in a Coaxial Hall Discharge Plasma," Physical Review E 63, 026410, 1-7 (2001).

[24] Meezan, N. B. and Cappelli, M. A., "Kinetic Study of Wall Collisions in a Coaxial Hall Discharge," Physical Review E 66, 036401, 1-10 (2002).

[25] Hagelaar, G. J. M., Bareilles, J., Garrigues, L., and Bouef, J. P., "Role of Anomalous Electron Transport in a Stationary Plasma Thruster Simulation," Journal of Applied Physics 93, 1, 67-75 (2003).

[26] Koo, J. W. and Boyd, I. D., "Modeling of Anomalous Electron Mobility in Hall Thrusters," Physics of Plasmas 13, 033501 (2006).

[27] Linnell, J. A., "An Evaluation of Krypton Propellant in Hall Thrusters," Ph.D. Dissertation, Aerospace Engineering, University of Michigan, 2007.

[28] Adam, J. C., Heron, A., and Laval, G., "Study of Stationary Plasma Thrusters Using Two-Dimensional Fully Kinetic Simulations," Physics of Plasmas 11, 1, 295-305 (2004).

[29] Boniface, C., Garrigues, L., Hagelaar, G. J. M., Bouef, J. P., Gawron, D. et al., "Anomalous Cross Field Electron Transport in a Hall Effect Thruster," Applied Physics Letters 89, 161503 (2006).

[30] Garrigues, L., Hagelaar, G. J. M., Boniface, C., and Bouef, J. P., "Anomalous Conductivity and Secondary Electron Emission in Hall Effect Thrusters," Journal of Applied Physics 100, 123301 (2006).

[31] Kaganovich, I., Raitses, Y., and Sydorenko, D., "Electron Kinetic Effects and Beam-Related Instabilities in Hall Thrusters," Presented at the 30th International Electric Propulsion Conference, IEPC Paper 2007-052, Florence, Italy, Sept. 17-20, 2007.

[32] Sydorenko, D., Smolyakov, A., Kaganovich, I., and Raitses, Y., "Modification of Electron Velocity Distribution in Bounded Plasmas by Secondary Electron Emission," IEEE Transactions on Plasma Science 34, 3, 815-824 (2006).

[33] Ducrocq, A., Adam, J. C., Heron, A., and Laval, G., "High-Frequency Electron Drift Instability in the Cross-Field Configuration of Hall Thrusters," Physics of Plasmas 13, 102111 (2006).

[34] Lazurenko, A., Vial, V., Prioul, M., and Bouchoule, A., "Experimental Investigation of High-Frequency Drifting Perturbations in Hall Thrusters," Physics of Plasmas 12, 013501 (2005).

[35] Lazurenko, A., Albarede, L., and Bouchoule, A., "Physical Characterization of High-Frequency Instabilities in Hall Thrusters," Physics of Plasmas 13, 083503 (2006).

[36] Lazurenko, A., Dudok de Wit, T., Cavoit, C., Krasnoselskikh, V., Bouchoule, A. et al., "Determination of the Electron Anomalous Mobility through Measurements of Turbulent Magnetic Field in Hall Thrusters," Physics of Plasmas 14, 033504 (2007).

[37] Lazurenko, A., Coduti, G., Mazouffre, S., and Bonhomme, G., "Dispersion Relation of High-Frequency Plasma Oscillations in Hall Thrusters," Physics of Plasmas 15, 034502 (2008).

[38] Kozlov, V. I., "Electron Dynamics after Exit Plane of Stationary Plasma Thruster Discharge Chamber," Journal of Propulsion and Power 24, 4, 842 (2008).

[39] Reid, B. M. and Gallimore, A. D., "Plasma Potential Measurements in the Discharge Channel of a 6-kW Hall Thruster," AIAA Paper 2008-5185, July 2008.

[40] Cappelli, M. A., Meezan, N. B., and Gascon, N., "Transport Physics in Hall Plasma Thrusters," AIAA Paper 2002-0485, Jan. 2002.

[41] Scharfe, M. K., Thomas, C. A., Scharfe, D. B., Gascon, N., Cappelli, M. A. et al., "Shear-Based Model for Electron Transport in Hybrid Hall Thruster Simulations," IEEE Transactions on Plasma Science (accepted for publication, 2008).

[42] Fox, J. M., "Advances in Fully-Kinetic PIC Simulations of a near-Vacuum Hall Thruster and Other Plasma Systems," Ph.D. Dissertation, Aeronautics and Astronautics, Massachusetts Institute of Technology, 2007.

[43] Garrigues, L., Boyd, I. D., and Boeuf, J. P., "Computation of Hall Thruster Performance," Journal of Propulsion and Power 17, 4, 772 (2001).

[44] Reid, B. M., Shastry, R., Gallimore, A. D., and Hofer, R. R., "Angularly-Resolved ExB Probe Spectra in the Plume of a 6-kW Hall Thruster," AIAA Paper 2008-5287, July 2008.

[45] Shastry, R., Hofer, R. R., Reid, B. M., and Gallimore, A. D., "Method for Analyzing ExB Probe Spectra from Hall Thruster Plumes," AIAA Paper 2008-4647, July 2008.

[46] Hofer, R. R. and Gallimore, A. D., "High-Specific Impulse Hall Thrusters, Part 2: Efficiency Analysis," Journal of Propulsion and Power 22, 4, 732-740 (2006).

[47] Bareilles, J., Hagelaar, G. J. M., Garrigues, L., Boniface, C., and Boeuf, J. P., "Critical Assessment of a Two-Dimensional Hybrid Hall Thruster Model: Comparisons with Experiments," Physics of Plasmas 11, 6, 3035 (2004).

[48] Dugan, J. V. and Sovie, R. J., "Volume Ion Production Costs in Tenuous Plasmas," NASA Lewis Research Center, NASA TN D-4150, September 1967.

[49] Jameson, K. K., "Investigation of Hollow Cathode Effects on Total Thruster Efficiency in a 6 kW Hall Thruster," Ph.D. Dissertation, Aerospace Engineering, University of California, Los Angeles, 2008.

[50] Jameson, K. K., Goebel, D. M., Hofer, R. R., and Watkins, R. M., "Cathode Coupling in Hall Thrusters," Presented at the 30th International Electric Propulsion Conference, IEPC Paper 2007-278, Florence, Italy, Sept. 17-20, 2007.

[51] Reid, B. M. and Gallimore, A. D., "Langmuir Probe Measurements in the Discharge Channel of a 6-kW Hall Thruster," AIAA Paper 2008-4920, July 2008.

[52] Brown, D. L., Larson, C. W., Haas, J. M., and Gallimore, A. D., "Analytical Extraction of Plasma Properties Using a Hall Thruster Efficiency Architecture," IEPC Paper 2007-188, Sept. 2007.

[53] Brown, D. L., Larson, C. W., Hargus, W. A., and Gallimore, A. D., "Standardization of Hall Thruster Efficiency Analysis: Methodology and Historical Perspective," AIAA Journal (submitted for publication, 2008).

[54] Ahedo, E. and Parra, F. I., "Partial Trapping of Secondary-Electron Emission in a Hall Thruster Plasma," Physics of Plasmas 12, 073503 (2006).

[55] Mc Eachran, R. P. and Stauffer, A. D., "Elastic Scattering of Electrons from Krypton and Xenon," J. Phys. B: At. Mol. Phys. 17, 2507-2518 (1984).

[56] Huba, J. D., *NRL Plasma Formulary*. (Naval Research Laboratory, Washington, DC, 2007).

[57] Hofer, R. R., "Development and Characterization of High-Efficiency, High-Specific Impulse Xenon Hall Thrusters," Ph.D. Dissertation, Aerospace Engineering, University of Michigan, 2004. (Also NASA/CR-2004-213099)

[58] Goebel, D. M. and Katz, I., *Fundamentals of Electric Propulsion: Ion and Hall Thrusters*. (John Wiley & Sons, New York, 2007).